Influence of confining pressure-dependent Young's modulus on the convergence of underground excavation

Xuezhen Wu[1], Yujing Jiang[2,*], Zhenchang Guan[1], Bin Gong[2]

[1]*College of Civil Engineering, Fuzhou University, Fuzhou 350108, China;*

[2]*Graduate School of Engineering, Nagasaki University, Nagasaki 852-8521, Japan.*

Corresponding author: Yujing Jiang

Email: jiang@nagasaki-u.ac.jp

Corresponding Address: Bunkyo Machi 1-14, Nagasaki 852-8521, Japan.

Phone: +81-080-3118-5202 Fax: +0532-86057957

Influence of confining pressure-dependent Young’s modulus on the convergence of underground excavation

ABSTRACT: The actual convergence of an excavation located in fractured rock mass or the soft rock is largely different with the theoretical result in many cases. Experimental results showed that the influence of confining pressure on Young's modulus is very significant. This paper attempted to illustrate the influence of the confining pressure-dependent Young’s modulus in the ground reaction analyses of mountain tunnel. Firstly, the relationship between Young's modulus and confining pressure was described as a non-linear function according to the test results. Based on the plane strain axial symmetry assumption and the incremental theory of plasticity, equilibrium equations and compatibility equations of rock mass around a circular tunnel were deduced theoretically. Based on fourth Runge-Kutta method, a semi-analytical solution was achieved. Considering the effect of confining pressure on Young's modulus, the stress and deformation of rock mass around tunnel was calculated by both analytical and numerical methods. The influence of confining pressure-dependent Young’s modulus in surrounding rock was estimated quantitatively. Finally, Tawara saka Tunnel in Japan was taken as an example to explain the influence of confining pressure-dependent Young’s modulus. The results showed that the error with respect to the monitoring data was largely reduced with the confining pressure-dependent Young’s modulus model, which indicated the necessity of considering the non-uniform distribution of Young’s modulus.

Keywords: Young’s modulus; confining pressure; semi-analytical solution; numerical simulation; underground excavation

1. Introduction

In engineering practice, the analytical and numerical methods are inevitably required to estimate the stress and deformation of surrounding rock mass and to help the design of support system (Li et al., 2008; Huang et al., 2015; Zhang et al., 2015; Feng et al., 2017; Wu et al., 2018a). However, the actual convergence of an excavation located in fractured rock mass or soft rock was largely different with the theoretical results in many cases. Accurate rock parameters and constitutive model are indispensable for the convergence and stability evaluation by analytical and numerical methods. The confining pressure effect on rock strength and Young's modulus should to be considered (Hsieh et al., 2014; Cai et al., 2015).

The influence of confining pressure on rock strength has been studied in depth. Many constitutive models considering confining pressure effect has been established (Fang and Harrison, 2001; Alejano et al., 2009). Cui at al. (2015) conducted an elasto-plastic analysis of a circular opening in rock mass with confining stress-dependent strain-softening behaviour. Moreover, Zhang at al. (2018) obtained an elastoplastic coupling solution of circular openings in strain-softening rock mass considering pressure-dependent effect.

The non-uniform distribution of Young's modulus is considered as another important factor. However, there are relatively few studies about the confining pressure effect on the Young's modulus. Numerous papers were contributed to the determination of Young's modulus of rocks (Palmstrom et al., 2001; Isik et al., 2008; Kodama et al., 2013; Agan et al., 2014; Tinoco et al., 2014). Some of them were focused on the relationship of the Young's modulus and the uniaxial compressive strength (UCS), rock mass rating (RMR) and geological strength index (GSI) for different type of rocks (Leite et al., 2001; Gokceoglua et al., 2003; Kayabasi et al., 2003; Karakus et al., 2005; Hoek et al., 2006; Feng et al., 2014).

Some other works were concentrated on the laboratory experiment to verify the confining pressure effect on the Young's modulus, and some empirical equations were obtained (You et al., 2003; Arslan et al., 2008; Wang et al., 2009; Cai et al., 2015; Yang et al., 2016). However, the attempt to describe the exact influence of the confining pressure-dependent Young's modulus of rock mass in the ground reaction analyses is quite few.

Brown et al. (1989) presented a stress-dependent elastic moduli and obtained the stresses around the axisymmetric boreholes. It was the earliest literature proposing exponential function of pressure-dependent young's modulus. Nawrocki et al. (1995) studied the damaged zones around openings using radius-dependent Young's modulus by numerical simulation. Zhang et al (2012) obtained a closed-form solution for circular openings modeled by the Unified Strength Theory and radius-dependent Young's modulus. This contribution was the first step in obtaining an analytical solution that considers the effect of confining pressure on the Young's modulus. While, the modulus was defined as a direct function of radius rather than the confining pressure, which was not exactly conform to the actual behaviour of surrounding rock mass. Therefore, more work need to be done to get an analytical solution for circular openings considering confining pressure-dependent Young's modulus.

In engineering practice, the distribution of confining pressure is very complex (Jiang et al., 2001). For a general excavation, the confining pressure (minor principal stress) acting on the excavation surface is zero. It increases gradually with the increasing distance between the element and the excavation surface, and will reach a constant value at locations far away from the excavation (Carranza et al., 1999; Hasanpour et al., 2015). Hence, it is necessary to consider the stress field change in the rock mass surrounding the excavation to accurately predict the ground response, especially in deep buried excavations.

Considering the effect of the confining pressure on Young's modulus, the stress and deformation of rock mass around a circular tunnel were calculated by both analytical and numerical methods. The influence of the confining pressure-dependent Young's modulus in surrounding rock was estimated quantitatively in the ground reaction analyses.

2. Relation of confining pressure and Young's modulus

Generally, the Young's modulus of rock mass was often assumed to be uniform in the ground reaction analyses (Graziani et al., 2005; Hasanpour et al., 2015). However, it was observed that the Young's modulus around an excavation was not constant, but rather non-uniform (Zhang et al., 2012; Cai et al., 2015). The Young's modulus of rock mass depends on many factors such as rock quality and confinement. In particular, confinement has a large influence on the Young's modulus. Hence, the stress redistribution due to excavation has a profound influence on the Young's modulus in underground engineering.

Based on a large amount of laboratory test results, You et al., (2003) pointed out that high confining pressure influence the Young's modulus of specimen from weathered rock or weak rock significantly. The relationship between confining stress and Young's modulus for rock masses was approximate to be exponent dependence. The increasing of fiction in the fissures with confining pressure reduces the shear slide, which makes Young's modulus higher.

To obtain a general function to describe the non-linear Young's modulus model, Cai et al. selected four sets experimental data of different rocks (Meglis et al.,1996; He et al., 2006; Mohammad et al., 2013; Cai et al., 2015), and get the best-fit curves. Fig. 1 presented the relationship between the confining pressure and the Young's modulus for the selected test data and the best-fit curves using the non-linear weighted fitting method. The best-fit equations that correspond to different rocks were also shown in Fig. 1.

Based on the fitting results, the non-linear model of Young's modulus and minor principal stress was shown in Fig. 2. A non-linear function was proposed to describe the relationship between the Young's modulus E and confining pressure σ_3 (Cai et al., 2015):

$$E = E_{max} - (E_{max} - E_0)\, e^{(-a^* \sigma_3)} . \quad (1)$$

where E_{max} is the maximum Young's modulus at the critical confining pressure, E_0 is the Young's modulus at no confining condition, and a is a model constant. This function can describe the curves very well for rock masses at non-uniform confinement condition. The physical meaning of the properties in Eq. (1) is clear. E_{max} can be considered as the Young's modulus of rock mass at in-situ stress state; E_0 can be viewed as the minimum Young's modulus at the excavation surface, and a controls the non-linearity of the curve and it varies for different rock masses. The influence of model constant a will be discussed later.

As the confining pressure could influence the Young's modulus dramatically, it was necessary to estimate the influence of the non-linear Young's modulus model on the deformation and failure characteristics of rock mass near excavation boundaries. Because of the lacking of well controlled in-situ experiments, field data was rarely available to determine the influence of the non-linear Young's modulus. Fortunately, the development of semi-analytical and numerical methods based on the computer makes it possible to estimate the influence of the confining pressure-dependent Young's modulus in surrounding rock quantitatively in the ground reaction analyses.

3. Ground reaction analyses of a circular tunnel with confining pressure-dependent Young's modulus model

The confining pressure-dependent Young's modulus model was applied in the ground reaction analyses of a circular tunnel to reveal its influence on the tunnel convergence.

3.1. Problem description

The excavation of long deep tunnels with circular cross section under hydrostatic in-situ stress condition could be considered as an axial symmetry plane strain problem, while neglecting the influence of gravity, and restricting the out-of-plane principal stress as intermediate stress (Li et al., 2013; Mohamad et al., 2013). The geomechanics sign convention was employed, and the radial displacement towards tunnel axis was taken as positive consequently. The stress and displacement redistributions (or namely ground responses) after excavation were evaluated with different Young's modulus models.

3.2. Equilibrium equations for rock mass

Consider an infinitesimal volume in the radial direction as shown in Fig. 3. The rock mass is subjected to a radial stress σ_r, a tangential stress σ_t. The static equilibrium condition of the infinitesimal rock mass volume can be formulated as:

$$\sigma_r r d\omega L_z + 2\sigma_t dr L_z \sin\frac{d\omega}{2} = (\sigma_r + d\sigma_r)(r + dr)d\omega L_z \,. \tag{2}$$

where, r is the radius of the infinitesimal volume, $d\omega$ is the loop angle, dr is the size in the radial direction, L_z is the size in the axial direction of the tunnel. It is clear that the confining pressure is the radial stress for a circular symmetric tunnel. Noticing that $\sin(\frac{d\omega}{2})$ approximately equals $\frac{d\omega}{2}$ since $d\omega$ is an infinitesimal, the equilibrium equation can be deduced as:

$$\frac{d\sigma_r}{dr} = \frac{\sigma_t - \sigma_r}{r} \,. \tag{3}$$

When applying Eq. (3) to the elastic region, where the stress state of rock mass should verify the hydrostatic in-situ stress condition that the sum of σ_r and σ_t equals $2P_0$, where P_0 is the in-situ stress. The equilibrium equation for elastic region can be formulated as:

$$\frac{d\sigma_r}{dr} = \frac{2P_0 - 2\sigma_r}{r} . \tag{4}$$

When applying it to the plastic region, where the stress state of rock mass should verify the Mohr–Coulomb failure criterion, the equilibrium equation for the plastic region can be formulated as:

$$\frac{d\sigma_r}{dr} = \frac{(K_p - 1)\sigma_r + \sigma_c}{r} . \tag{5}$$

Where, K_p is the passive coefficient and remains unchanged within the complete plastic region. K_p equals to (1+sin φ)/(1-sin φ), where φ is friction angle of rock. σ_c is the compression strength, which changes gradually from σ_c^1 to σ_c^2, according to the evolution of the major principal plastic strain ε_1^p.

$$\sigma_c = \begin{cases} \sigma_c^1 - \dfrac{(\sigma_c^1 - \sigma_c^2)\varepsilon_1{}^p}{\alpha\varepsilon_1^e} & (0 \le \varepsilon_1{}^p \le \alpha\varepsilon_1^e) \\ \sigma_c^2 & (\varepsilon_1{}^p \ge \alpha\varepsilon_1^e) \end{cases} . \tag{6}$$

where α is a softening parameter controlling the gradual transition of rock from a peak failure criterion to a residual one (Jiang et al., 2001; Alonsol et al., 2003; Guan et al., 2007).

3.3. Displacement compatibility equations for rock mass

Due to the plane strain axial symmetry assumption, the strain-displacement relationships for the rock mass can be simplified significantly as:

$$\frac{du}{dr} = \varepsilon_r \quad \frac{u}{r} = \varepsilon_t . \tag{7}$$

In the elastic region, according to Hook's law, the tangential strain of the rock mass can be evaluated from its stress state, as formulated in Eq. (8), where E and ν are the Young's modulus and the Poisson ratio of the rock mass. Here, E is a variable which is always changing with the confining pressure as shown in Eq. (1).

$$\varepsilon_t = (\frac{\sigma_t}{E} - \nu\frac{\sigma_r}{E} - \nu\frac{2P_0\nu}{E}) - (\frac{P_0}{E} - \nu\frac{P_0}{E} - \nu\frac{2P_0\nu}{E}) . \tag{8}$$

Notice that only the strain caused by tunnel excavation is concerned, which means the initial strain due to in-situ stresses should be removed. Then, associating these two equations and considering the hydrostatic in-situ stress condition, the displacement compatibility equation for the elastic region can be formulated as Eq. (9).

$$u = r\varepsilon_t = \frac{P_0 - \sigma_r}{E}(1+\nu)r \,. \tag{9}$$

For the plastic region, the incremental theory of plasticity (Graziani et al., 2005) is adopted, and the loading path refers to a monotonic decrease of the fictitious inner pressure, corresponding to the advancing of the tunnel face. Consequently, the rates of all mechanical variables can be evaluated by their first-order derivatives with respect to P_i. The total strain rate consists of both elastic part and plastic part, as shown in Eq. (10). The elastic part is controlled by Hooke's law and the plastic part by the potential flow rule, as formulated by Eqs. (11) and (12), respectively. The relationship between the strain rate and the displacement velocity is simplified by virtue of axial symmetry and formulated by Eq. (13).

$$\dot{\varepsilon}_r = \dot{\varepsilon}_r{}^e + \dot{\varepsilon}_r{}^p, \qquad \dot{\varepsilon}_\theta = \dot{\varepsilon}_\theta{}^e + \dot{\varepsilon}_\theta{}^p, \tag{10}$$

$$\dot{\varepsilon}_r{}^e = \frac{1-\nu}{2G}\dot{\sigma}_r - \frac{\nu}{2G}\dot{\sigma}_\theta, \quad \dot{\varepsilon}_\theta{}^e = \frac{1-\nu}{2G}\dot{\sigma}_\theta - \frac{\nu}{2G}\dot{\sigma}_r, \tag{11}$$

$$\dot{\varepsilon}_r{}^p = \lambda\frac{\partial g}{\partial \sigma_r} = \lambda, \quad \dot{\varepsilon}_\theta{}^p = \lambda\frac{\partial g}{\partial \sigma_\theta} = -\lambda K_\psi, \tag{12}$$

$$\dot{\varepsilon}_r = \frac{\partial \dot{u}}{\partial r}, \quad \dot{\varepsilon}_\theta = \frac{\dot{u}}{r}\,. \tag{13}$$

Here, g is the plastic potential. The rates of all mechanical variables (denoted by a dot mark) are referred as their first-order derivatives with respect to P_i. Then associating these four equations, eliminating the multiplier λ, the displacement compatibility equation for the plastic region can be expressed as:

$$\frac{\partial \dot{u}}{\partial r} + K_\psi\frac{\dot{u}}{r} = \frac{(1-\nu-\nu K_\psi)}{2G}\dot{\sigma}_r - \frac{(\nu K_\psi - K_\psi + \nu)}{2G}\dot{\sigma}_\theta\,. \tag{14}$$

3.4. Semi-analytical solution

As the Young's modulus E is a variable which is always changing with the confining pressure, it is impossible to get the rigid analytical solution. The displacement compatibility equation and the equilibrium equation could only be solved by semi-analytical methods. The fourth-order Runge-Kutta method (Basheer et al., 2000; Wu et al., 2018b.) was employed, and a two dimensional finite difference algorithm (i.e. along the unloading path and along the radial direction) was programed. All the variables describing the state of the surrounding rock mass have two indices: the first indicates a certain stage in the unloading path and the second indicates a certain position in the radial direction. Supposing that at former stage (say the $(k\text{-}1)^{\text{th}}$ stage where P_i=$P_i^{(k\text{-}1)}$), all the mechanical states of the rock mass were known, the objective was to evaluate all the mechanical states at current stage (i.e. the k^{th} stage where P_i=$P_i^{(k)}$) according to their known counterparts at the former stage, which included the following three steps: stress evaluation, displacement evaluation and parameters update. The parameters that need to be updated include the transitional strength and the Young's modulus of rock mass. After one iteration finished, these known mechanical states at the current stage could be used to evaluate the mechanical states at next stage, following the same three steps, and the iteration was repeated until the final stage.

3.4.1. Stress evaluation of rock mass

The equilibrium equations (4) and (5) were solved by the fourth-order Runge-Kutta method. The radial stress at the tunnel wall $\sigma_r(k, R_a)$ was known and equals to $P_i^{(k)}$, which served as the boundary condition of the equilibrium equations. When the radial stress increased up to the critical inner pressure P_i^{cri}, record the position as the radius of the elasto-plastic interface R_e, then go on evaluating the stress state of elastic region. The softening radius was obtained according to the major principal plastic strain ε_1^p. The detailed method can be found in existing literature (Guan et al. 2007). According to the research of Carranza-Torres et al., (1999), P_i^{cri} was a constant that only depends on the properties of rock mass itself and independent of the position of the elasto-plastic interface. The critical inner pressure can be calculated by the following formula.

$$P_i^{cri} = \sigma_{re} = \frac{2P_0 - \sigma_c}{K_p + 1}. \tag{15}$$

The radial and tangential stresses at the current stage could be determined after the stress evaluation process.

3.4.2. Displacement evaluation of rock mass

For the elastic region, the radial displacement of the rock mass could be evaluated directly by the radial stress of rock mass at the current stage, according to Eqs. (1) and (9). For the plastic region, the radial and tangential stress rates $\dot{\sigma}_r(k,r)$ and $\dot{\sigma}_t(k,r)$ should be first evaluated by their first-order difference with respect to P_i, as shown in Eq. (16).

$$\dot{\sigma}(k,r) = \frac{\sigma(k,r) - \sigma(k-1,r)}{dP_i} \quad (r \le R_e). \tag{16}$$

Similarly, the deformation rate at the elasto-plastic interface $\dot{u}(k,R_e)$, which served as the boundary condition of the compatibility equation, could also be obtained by its first-order difference with respect to P_i. Then the fourth-order Runge-Kutta method was utilized again to evaluate the deformation rate at each sequential calculation point (inward radial direction) according to the compatibility equations (14). Finally, the displacement at the current stage could be obtained by accumulating the displacement increment at the current stage to its counterpart at the former stage.

$$u(k,r) = u(k-1,r) + \dot{u}(k,r)dP_i \quad (r \le R_e). \tag{17}$$

The displacement and the stresses at the former stage, as well as the stresses at the current stage, were required during this step. Then the displacement at the current stage could be determined after the displacement evaluation process.

3.4.3. Rock mass parameters update

After the stress evaluation, the confining pressure (minimum principal stress) at the current stage was obtained. Then, the Young's modulus of rock mass at different locations at the current stage could be computed via Eq. (1).

After the displacement evaluation, the major principle plastic strain ε_t^p at the current stage, which served as the softening parameter herein, could be evaluated by Eq. (18). Then the transitional strength at the current stage could be computed via Eq. (6).

$$\varepsilon_t^p(k,r) = \varepsilon_t(k,r) - \varepsilon_{te}(k,r) = \frac{u(k,r)}{r} - \frac{u(k,R_e)}{R_e} \quad (r \le R_e). \tag{18}$$

The radial stress, tangential stresses and the displacement at the current stage were required in this step, and the Young's modulus and transitional strength of rock mass at the current stage can be determined. After these three steps, all the mechanical states at the current stage were known, which could be used to evaluate their counterparts at next stage.

4. Application and verification of the confining pressure-dependent Young's modulus model

The proposed method was programmed in Visual Basic development environment, and will be verified by numerical simulations in this section. In addition to Visual Basic, the available programming methods include C language, C++, Matlab, and many others. An illustrative case study was conducted to demonstrate the influence of confining pressure-dependent Young's modulus in conventional tunnelling.

4.1. An illustrative case study

Suppose that a circular tunnel with a design radius of 5.0 m was excavated under a hydrostatic in-situ stress of 40 MPa. The Young's modulus was assumed to transform from 20GPa (E_0) to 80GPa (E_{max}) with the increasing of confining pressure. The model constant a equaled to 0.05. The other properties of the rock mass employed were listed in Table 1.

The ground responses after excavation in the semi-analytical solution (including the distribution of stress, displacement, and Young's modulus) were shown in Fig. 4, Fig. 5, and Fig. 6 (represented by solid lines, Analytical_E_X). To highlight the influence of confining pressure-dependent Young's modulus, the ground responses with the constant Young's modulus model (Analytical_E_{20} and Analytical_E_{80}) were also calculated and depicted in these figures.

The semi-analytical results show that the stress distributions in the surrounding rock mass were almost the same for different models. The only difference lied in the softening region ($0 \le \varepsilon_1^p \le \alpha\varepsilon_1^e$). It is reasonable as the rock strength σ_c in this region is influenced by the major principal plastic strain ε_1^p as shown in Eq. 6. The displacement of rock mass is significantly affected by the confining pressure-dependent Young's modulus as shown in Fig. 5. The displacement with the new model falls between the two constant Young's modulus models, and more close to the 80GPa condition. Taking the maximum tunnel convergence as the estimation index, the error between the results of E_X and E_{80} is 49.26%, and the error between the results of E_X and E_{20} is 102.96%.

The Young's modulus distributions along the radial direction in the surrounding rock mass was shown in Fig. 6. The result shows that the Young's modulus increases nonlinearly with the increasing of radial distance. It is reasonable as the confining pressure (σ_r) increases with the increasing of radial distance and the Young's modulus is influenced by the confining pressure. The result also indicated that the new model is well expressed in the calculations. The influence rules of various parameters on the deformation and failure of rock mass will be revealed in the following parameters analysis.

4.2. Verification by numerical simulations

The validity of analytical method was verified by numerical simulations (codes: FLAC^{3D}). The strain-softening constitutive laws in FLAC^{3D} are characterized by six parameters: bulk modulus K, shear modulus G, friction angle ϕ, cohesion c, dilation angle ψ, and softening parameter η. It is obvious that the former five parameters can be evaluated directly from the parameters employed in the analytical method, via following relations:

$$K = \frac{E}{3(1-2\nu)}, \tag{19-1}$$

$$G = \frac{E}{2(1+\nu)}, \tag{19-2}$$

$$K_p = \frac{1+\sin\phi}{1-\sin\phi}, \tag{19-3}$$

$$\sigma_c = 2c\sqrt{K_p}, \tag{19-4}$$

$$K_\psi = \frac{1+\sin\psi}{1-\sin\psi}. \tag{19-5}$$

Where, K_ψ is the dilation factor, and equals to K_ψ^1 and K_ψ^2 for softening region and residual region, respectively.

However, the softening parameter in FLAC^{3D} is defined as shown in Eq. 20-1:

$$\delta\eta_{Flac} = \frac{1}{\sqrt{2}}\sqrt{(\delta\varepsilon_1{}^p - \delta\varepsilon_m{}^p)^2 + (\delta\varepsilon_m{}^p)^2 + (\delta\varepsilon_3{}^p - \delta\varepsilon_m{}^p)^2} \quad \text{with} \quad \delta\varepsilon_m^p = \frac{\delta\varepsilon_1^p + \delta\varepsilon_3^p}{3}. \tag{20-1}$$

Therefore, the shift point of the softening parameter in FLAC^{3D} can be obtained from the parameters used in the analytical method by:

$$\eta_{Flac}^{s} = \frac{\alpha}{\sqrt{3}}\sqrt{K_{\psi}^{2} + K_{\psi} + 1}\,. \tag{20-2}$$

The confining pressure-dependent Young's modulus model used in the semi-analytical method cannot be directly simulate by the default model in $FLAC^{3D}$. Fortunately, it provides a user-defined programming language FISH, which can adjust the Young's modulus according to the stress state of every element after every step. Then the modified Young's modulus is used in the next cycling of $FLAC^{3D}$.

Because of the symmetry conditions, only one-fourth of the tunnel was modeled. The thickness of the numerical model is 1 m. The lower boundary was fixed in the y-direction. The left boundary was fixed in the x-direction. A vertical stress of 40 MPa was applied at the top boundary. A horizontal stress of 40 MPa was applied at the right boundary. The gravitational stress-gradient was not considered in this analysis.

The results from the numerical simulations were also depicted in Figs. 4-6, as denoted by triangle, cross and circle marks for three different cases respectively. As shown in these figures, the ground responses computed by the analytical method and by the numerical simulation fit each other exactly for the most part, indicating that the semi-analytical solutions for the new model in the circular tunnel was valid. In addition, the Young's modulus contour around the tunnel in numerical result is shown in Fig. 6b.

5. Parameters analysis

Parameters analysis was conducted to study the influence of different parameters in the confining pressure-dependent Young's modulus model. The studied parameters included the maximum Young's modulus (E_{max}), the minimum Young's modulus (E_0), and the model constant a. The semi-analytical method was adopted in this part as the calculation can be finished in a few seconds. While, a lot of time is needed in numerical method to get the similar results. The maximum tunnel convergence was selected as the estimation index in this study. Taking the illustrative case above as a standard one and varying a single parameter, the relative significance of different parameters on the deformation characteristics of rock mass will be illustrated.

5.1. Influence of the maximum Young's Modulus

The maximum Young's modulus (E_{max}) was selected to study its influence on the tunnel convergence. As the minimum Young's modulus (E_0) is 20GPa in the standard case, the E_{max} is set from 20GPa to 100GPa in the following studies. Meanwhile, the other parameters are all the same with the standard case.

The evolution of the maximum displacement with the increasing of maximum Young's modulus was shown in Fig. 7. To highlight the difference, the results of constant Young's modulus model (E_0 and E_{max}) were also calculated and depicted in this figure. The results show that the maximum displacement in the new model decreases gradually with the increasing of E_{max}. Similar behaviour was found in the case of constant Young's modulus model when the Young's modulus equals to E_{max}. In the case of constant Young's modulus model when the Young's modulus equals to E_0, the maximum displacement doesn't change. When the E_{max} is very small, the difference between E_{max} and E_0 is very small, which certainly resulting in small difference for different models.

5.2. Influence of the minimum Young's Modulus

The influence of the minimum Young's modulus E_0 was studied in this part. As the maximum Young's modulus E_{max} is 80GPa in the standard case, E_0 was set from 10GPa to 80GPa in the following examples. The other parameters were also the same with the standard case. The evolution of the maximum displacement with the increasing of E_0 were shown in Fig. 8.

The results show that the maximum displacement decreases sharply with the increasing of E_0 in the case of constant Young's modulus E_0. The displacement with the new model always falls between the two constant Young's modulus models. When the value of E_0 is close to E_{max}, the difference between the three cases is also small. The result illustrates that the difference between E_{max} and E_0 is a key parameter that influence the error between the confining pressure-dependent Young's modulus model and uniform Young's modulus model.

5.3. Influence of the model constant

The influence of model constant (a) was studied in this part. It was set from 0.001 to 1 in the following examples. The other parameters were also same with the standard case. The evolution of the maximum displacement with the increasing of model constant are shown in Fig. 9. The results of two constant Young's modulus models were also depicted in this figure.

The results show that the maximum displacement from the new model decreases gradually with the increasing of model constant. There is a clearly trend that the maximum displacement from the confining pressure-dependent Young's modulus model gradually approaching the E_{max} case from the E_0 case with the increasing of model constant. This behaviour can be explained by the distribution of Young's modulus with different value of model constant as shown in Fig. 10. The results above show that the confining pressure-dependent Young's modulus of rock mass influences the tunnel convergence dramatically, which shouldn't be ignored.

6. Predicting the deformation of surrounding rock mass in tunnel construction

6.1. Geological and excavation conditions of Tawara saka tunnel

The excavation of Tawara saka Tunnel on Kyushu Shinkansen in Nagasaki was taken as an example to explain the influence of confining pressure-dependent Young's modulus. The tunnel convergence at the position of 16.074km from Takeo Onsen was discussed in detail. Its buried depth is 234.9 m. There are two types of rocks around the tunnel as shown in Fig. 11. The geological investigations and the laboratory experimental results show that the strength of the rock around the tunnel is very low, and both of them are classified as DII, which belongs to the classification of the soft rock.

The dimensions of cross section and the monitoring positions for tunnel convergence, mainly including the convergence at the crown (u_c) and at 1m above the springline (u_{sr} and u_{sl}), were schematically illustrated in Fig. 12. The standard supporting pattern in Japan was adopted. The upper stage was excavated first, and then the first lining and the rock bolts were installed immediately. After that, the displacement meters were installed and started to monitor the tunnel convergence. Then, the lower stage was excavated and supported similarly. The second lining was cast in place a few days later. The internal pressure of the support structure on the rock mass is determined to be 0.817MPa according to the monitoring data of pressure cell.

6.2. Numerical simulation to predict the tunnel convergence

A numerical model (codes: $FLAC^{3D}$) including five groups was established as shown in Fig. 11b, including three groups in the tunnel to be excavated and two groups to stand for the different rocks. Both of the rocks are assumed as Mohr-Coulomb materials. The properties of both rocks are listed in Table 2. The parameters were identified by laboratory tests. The confining pressure-dependent Young's modulus model here is also characterized by adjust the Young's modulus according to the stress state of every element.

In the numerical simulation, the groups 1 and 2 were set to be null after the initial state, and then an internal pressure of 70% in situ stress was applied on the tunnel surface to simulate the support effect of the rock mass ahead of the tunnel face and the support structure. After the balance of the calculation model, the displacement were initialed to correspond to the in situ monitoring data. Then, the group 3 was set to be null, and an internal pressure was applied on the tunnel surface. Finally, the internal pressure was reduced gradually to simulate the advance of tunnel face. According to the monitoring data of pressure cell, the internal pressure was identified to be 0.817MPa to replace the effect of support.

The results from the numerical simulations by two methods were shown in Fig. 13 and Fig. 14 respectively. The maximum displacement from different numerical methods were compared with the monitoring data in Fig. 15. All the displacements shown in Fig. 15 was ten times magnified with respect to the original data to demonstrate the difference more clearly. The quantitative data was shown in Table 3. The maximum displacements of the tunnel for three monitoring points were also shown in Table 3. The errors of maximum tunnel displacement with different methods compared with the monitoring data was analyzed in Table 4.

Both the numerical results show that the tunnel convergence is unsymmetrical, which is consistent with the monitoring data. The displacement at the left side is much larger than the right side. This is reasonable as the rock strength and Young's modulus of the left part is much smaller than the right side.

The tunnel convergence computed from the confining pressure-dependent Young's modulus model is smaller than that from the uniform Young's modulus model, and more close to the field test data. The error analysis shows that the error with respect to the monitoring data is largely reduced with the confining pressure-dependent Young's modulus model in most part. The data at 1m above the springline fits much better than the monitoring position of tunnel crown. May be the relative sliding between the two types of rock mass happened in situ, which result in a large displacement in the X direction. While, this behaviour is not occurred as the bond between the two types of rock mass is too strong in the laboratory test.

As the other properties of rock mass, such as the residual strength and dilation angle, are also influenced by the confining pressure, which are not considered in these simulations may be the reason of the slight errors. Nevertheless, the simulation results indicate that it is necessary to consider the confining pressure-dependent of Young's modulus in rock mass around the tunnel.

7. Conclusions

According to test data and research achievement available in literature, the relationship between Young's modulus and confining pressure was described as a non-linear function. In an underground excavation, the confining pressure acting on an element is a function of distance between the element and the excavation boundary. Since the Young's modulus is depended on the confining pressure, it is necessary to consider the stress field change in the rock mass surrounding the excavation to accurately predict the ground response, especially in deep buried excavations.

Based on the plane strain axial symmetry assumption and the incremental theory of plasticity, equilibrium equations and compatibility equations of rock mass around a circular tunnel were deduced theoretically. Based on fourth Runge-Kutta method, a semi-analytical solution was achieved through programming. In the calculation, the Young's modulus of rock mass was real-time updated according to the local confining pressure.

Considering the effect of the confining pressure on the Young's modulus, the stress and deformation of rock mass was calculated in the ground reaction analyses by both analytical and numerical methods. The influence of the confining pressure-dependent Young's modulus in surrounding rock was estimated quantitatively. Taking the maximum tunnel convergence as the estimation index, the error between the results of confining pressure-dependent Young's modulus model and two uniform Young's modulus models were 49.26% and 102.96%.

Parameters analysis were conducted to study the influence of the maximum Young's modulus (E_{max}), the minimum Young's modulus (E_0), and the model constant a in the confining pressure-dependent Young's modulus model. The result illustrated that the difference between E_{max} and E_0 is a key parameter that influence the error between the confining pressure-dependent Young's modulus model and uniform Young's modulus model. There is a clearly trend that the maximum displacement from the confining pressure-dependent Young's modulus model gradually approaching the E_{max} case from the E_0 case with the increasing of model constant.

Finally, the Tawara saka Tunnel on Kyushu Shinkansen was taken as an example to explain the influence of the confining pressure-dependent Young's modulus. A numerical model with two different types of rock mass was established to simulate the tunnel behaviour after excavation. Both of the numerical results showed that the tunnel convergence was unsymmetrical, which was consistent with the monitoring data. The error analysis showed that the error with respect to the monitoring data was largely reduced with the confining pressure-dependent Young's modulus model. The simulation results indicated that it is necessary to consider the non-uniform distribution of Young's modulus in rock mass around the tunnel.

Acknowledgments

This study was funded by the National Natural Science Foundation of China (No. 51379117).

References

Agan, C., 2014. Determination of the deformation modulus of dispersible-intercalated-jointed cherts using the Menard pressuremeter test. Int. J. Rock Mech. Min. Sci. 65, 20–28.

Alejano, L.R., Rodriguez, D.A., Alonso, E., Fdez-Manin, G., 2009. Ground reaction curves for tunnels excavated in different quality rock masses showing several types of post-failure behaviour. Tunn. Undergr. Sp. Technol. 24, 689–705.

Alonsol, E., Alejano, L.R., Varas, F., Fdez-Manin, G., and Carranza-Torres, C., 2003. Ground response curves for rock masses exhibiting strain-softening behaviour. Int. J. Numer. Anal. Met. 27, 1153–1185.

Arslan, A.T., Koca, M.Y., Aydogmus, T., Klapperich, H., and Yılmaz, H.R., 2008. Correlation of Unconfined Compressive Strength with Young's Modulus and Poisson's Ratio in Gypsum from Sivas (Turkey). Rock Mech. Rock Eng. 41, 941–950.

Basheer, I., and Hajmeer, M., 2000. Artificial neural network: fundamentals, computing, design and application. J. Microbiol. Meth. 43, 3–31.

Brown, E.T., Bray, J.W., Santarelli, F.J., 1989. Influence of stress-dependent elastic moduli of stresses and stresses around axisymmetric boreholes. Rock Mech. Rock Eng. 22: 189-203.

Cai, M., and Wang, X., 2015. A non-uniform velocity model and Flac/Specfem2d coupled numerical simulation of wave propagation in underground mines. 13th ISRM International Congress of Rock Mechanics, Montreal, May 10–13, p. 1–17

Carranza, T.C., and Fairhurst, C., 1999. The elasto-plastic response of underground excavations in rock masses that satisfy the Hoek-Brown failure criterion. Int. J. Rock Mech. Min. Sci. 36, 777–809.

Cui, L., Zheng, J.J., Zhang, R.J., Dong, Y.K., 2015. Elasto-plastic analysis of a circular opening in rock mass with confining stress-dependent strain-softening behaviour, Tunnel. Undergr. Space Technol. 50, 94-108.

Fang, Z., Harrison, J.P., 2001. A mechanical reduction index for rock. Int. J. Rock. Mech. Min. Sci. 38(8), 1193–1199.

Feng, X.D., and Jimenez, R., 2014. Bayesian prediction of elastic modulus of intact rocks using their uniaxial compressive strength. Eng. Geol. 173, 32–40.

Feng, X.T., Pei, S.F., Jiang, Q., Zhou, Y.Y., Li, S.J., Yao, Z.B., 2017. Deep fracturing of the hard rock surrounding a large underground cavern subjected to high geostress: in situ observation and mechanism analysis. Rock Mech Rock Eng. 50, 2155–2175.

Gokceoglua, C., Sonmeza, H., and Kayabasi, A., 2003. Predicting the deformation moduli of rock masses. Int. J. Rock Mech. Min. Sci. 40, 701–710.

Graziani, A., Boldini, D., and Ribacchi, R., 2005. Practical estimate of deformations and stress relief factors for deep tunnels supported by shotcrete. Rock Mech. Rock Eng. 38, 345–372.

Guan, Z., Jiang, Y., and and Tanabasi, Y., 2007. Ground reaction analyses in conventional tunneling excavation. Tunnel. Undergr. Space Technol. 22, 230–237.

Hasanpour, R., Rostami, J., and Barla, G., 2015. Impact of Advance Rate on Entrapment Risk of a Double-Shielded TBM in Squeezing Ground. Rock Mech. Rock Eng. 48, 1115–1130.

He, T.W., 2006. P- and S-wave velocity measurement and pressure sensitivity analysis of AVA response. Master thesis. University of Alberta, Alberta, Canada, 178 p.

Hoek, E., and Diederichs, M.S., 2006. Empirical estimation of rock mass modulus. Int. J. Rock Mech. Min. Sci. 43, 203–215.

Hsieh, A., Dyskin, A.V., and Dight, P., 2014. The increase in Young's modulus of rocks under uniaxial compression. Int. J. Rock Mech. Min. Sci. 70, 425–434.

Huang, H., Gong, W, Khoshnevisan, S., Juang, H., Zhang, D., Wang, L., 2015. Simplified procedure for finite element analysis of the longitudinal performance of shield tunnels considering spatial soil variability in longitudinal direction. Comput. Geotech. 64, 132–145.

Isik, N.S., Ulusay, R., and Doyuran, V., 2008. Deformation modulus of heavily jointed–sheared and blocky greywackes by pressuremeter tests: Numerical, experimental and empirical assessments. Eng. Geol. 101, 269–282.

Jiang, Y., Yoneda, H., and Tanabashi, Y., 2001. Theoretical estimation of loosening pressure on tunnels in soft rocks. Tunnel. Undergr. Space Technol. 16, 99–105.

Karakus, M., Kumral, M., and Kilic, O., 2005. Predicting elastic properties of intact rocks from index tests using multiple regression modelling. Int. J. Rock Mech. Min. Sci. 42, 323–330.

Kayabasi, A., Gokceoglub, C., and Ercanoglu, M., 2003. Estimating the deformation modulus of rock masses: a comparative study. Int. J. Rock Mech. Min. Sci. 40, 55–63.

Kodama, J., Miyamoto, T., Kawasaki, S., Fujii, Y., Kaneko, K., and Hagan, P., 2013. Estimation of regional stress state and Young's modulus by back analysis of mining-induced deformation. Int. J. Rock Mech. Min. Sci. 63, 1–11.

Leite, M.H., and Ferland, F., 2001. Determination of unconfined compressive strength and Young's modulus of porous materials by indentation tests. Eng. Geol. 59, 267–280.

Li, S.C., Cong, H., Li, L.P., Song, S.G., Zhou, Y., and Shi, S.S., 2013. Bidirectional construction process mechanics for tunnels in dipping layered formation. Tunnel. Undergr. Space Technol. 36, 57–65.

Li, S.C., Wang, M.B., 2008. Elastic analysis of stress–displacement field for a lined circular tunnel at great depth due to ground loads and internal pressure. Tunnel. Undergr. Space Technol. 23, 609–617.

Meglis, I.L., Greenfield, R.J., Engelder, T., and Graham, E.K., 1996. Pressure dependence of velocity and attenuation and its relationship to crack closure in crystalline rocks. J. Geophys. Res. 17, 523–517.

Mohamad, K., and Chang, Y.O., 2013. Evaluation of deformation parameter for deep excavation in sand through case histories. Comput. Geotech. 47, 57–67.

Mohammad, R.A., and Najibi, A.R., 2013. The effect of confining pressure on elastic wave velocities and dynamic to static Young modulus ratio. Geophysics, 78, 135–142.

Nawrocki, P.A., and Dusseault, M.B., 1995. Modelling of damaged zones around openings using radius-dependent Young's modulus. Rock Mech. Rock Eng. 28, 227–39.

Palmstrom, A., and Singh, R., 2001. The deformation modulus of rock masses-comparisons between in situ tests and indirect estimates. Tunnel. Undergr. Space Technol. 16, 115–131.

Tinoco, J., Correia, A.G., and Cortez, P., 2014. A novel approach to predicting Young's modulus of jet grouting laboratory formulations over time using data mining techniques.

Eng. Geol. 169, 50–60.

Wang, X.S., Jiang, X.W., Wan, L., Song, G., and Xia, Q., 2009. Evaluation of depth-dependent porosity and bulk modulus of a shear using permeability-depth trends. Int. J. Rock Mech. Min. Sci. 46, 1175–1181.

Wu X., Jiang Y., Li B., 2018a. Influence of joint roughness on the shear behaviour of fully encapsulated rock bolt. Rock Mech. Rock Eng. 51(3): 953–959.

Wu X., Jiang Y., Guan Z., Wang G., 2018b. Estimating the support effect of the energy-absorbing rock bolt based on the mechanical work transfer ability, Int. J. Rock Mech. Min. Sci. 103: 168-178.

Yang, J.P., Chen, W.Z., Yang, D.S., and Tian, H.M., 2016. Estimation of elastic moduli of non-persistent fractured rock masses. Rock Mech. Rock Eng. 49, 1977–1983.

You, M.Q., 2003. Effect of confining pressure on the Young's modulus of rock specimen and the friction in fissures. Rock and Soil Mechanics, S2, 167–170.

Zhang, C.G., Zhao, J.H., Zhang, Q.H., and Hu, X.D., 2012. A new closed-form solution for circular openings modeled by the Unified Strength Theory and radius-dependent Young's modulus. Comput. Geotech. 42, 118–128.

Zhang, J., Chen, H.Z., Huang, H.W., and Luo, Z., 2015. Efficient response surface method for practical geotechnical reliability analysis. Comput. Geotech. 69, 496–505.

Zhang, Q., Zhang C., Jiang B., Li N., Wang Y., (2018). Elastoplastic coupling solution of circular openings in strain-softening rock mass considering pressure-dependent effect. Int. J. Geomech. 18(1), 04017132.

FIGURE CAPTION

Figure 1. The Young's modulus versus confining pressure of the experimental data and best-fit curves (a) Waterford amphibolites, (b) Waterford gneiss, (c) Cadotte Sandstone, and (d) Sarvak limestone

Figure 2. The relationship of Young's modulus and confining pressure (minimum principal stress).

Figure 3. Static equilibrium condition for the surrounding rock mass.

Figure 4. The stress distributions in the surrounding rock mass.

Figure 5. The displacement distributions in the surrounding rock mass.

Figure 6. The Young's modulus distributions in the surrounding rock mass (a) analytical results, (b) numerical results.

Figure 7. The evolution of the maximum displacement with the increasing of Emax.

Figure 8. The evolution of the maximum displacement with the increasing of E0.

Figure 9. The evolution of the maximum displacement and the error with the increasing of model constant.

Figure 10. The distribution of Young's modulus with different value of model constant.

Figure 11. Tawara saka Tunnel at 16.074km (a) The exposed tunnel face, (b) Numerical model.

Figure 12. The cross section dimensions and the convergence monitoring positions.

Figure 13. Displacement of the rock mass around the tunnel by uniform Young's modulus model.

Figure 14. Displacement of the rock mass around the tunnel by non-uniform Young's modulus model.

Figure 15. Comparing of different numerical results with the monitoring data.

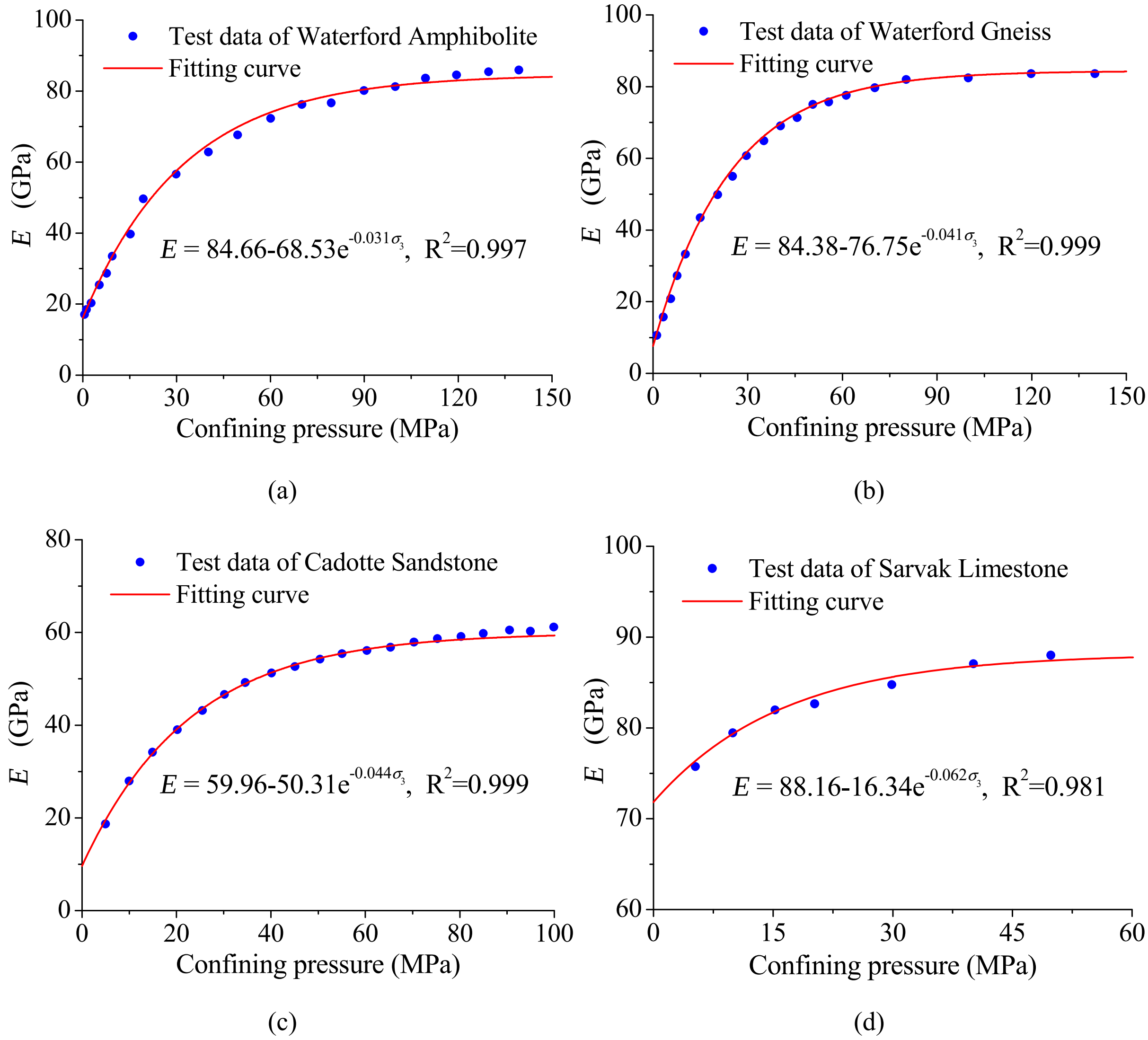

Fig. 1 The Young's modulus versus confining pressure of the experimental data and best-fit curves (a) Waterford amphibolites, (b) Waterford gneiss, (c) Cadotte Sandstone, and (d) Sarvak limestone

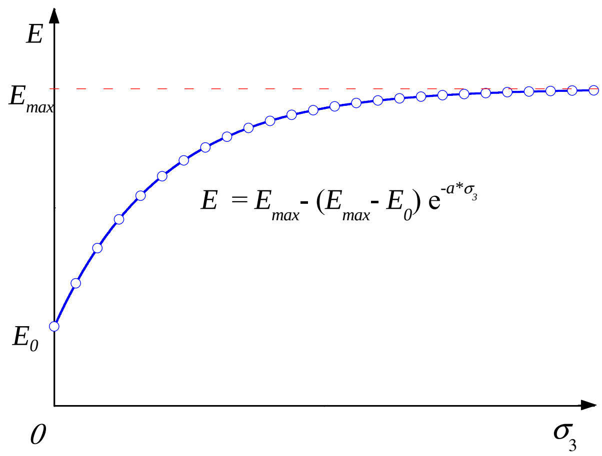

Fig. 2 The relationship of Young's modulus and confining pressure (minimum principal stress)

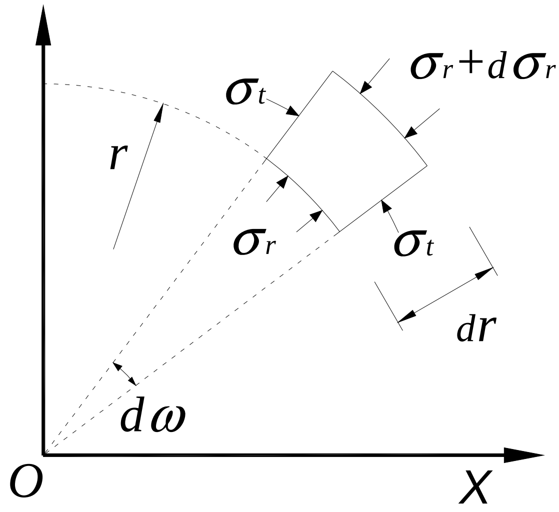

Fig. 3 Static equilibrium condition for the surrounding rock mass.

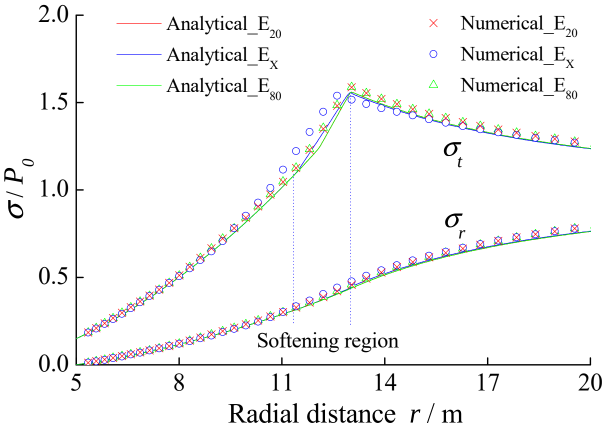

Fig. 4 The stress distributions in the surrounding rock mass

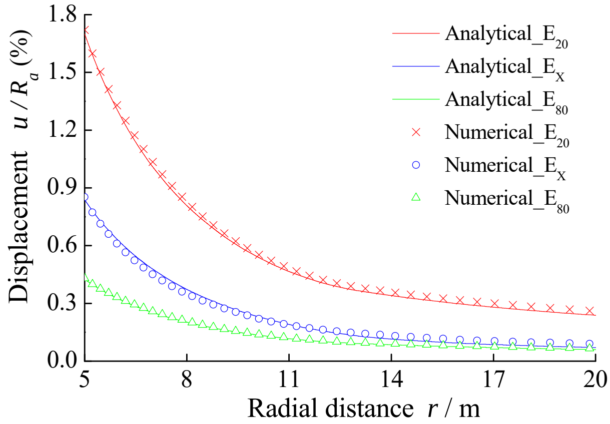

Fig. 5 The displacement distributions in the surrounding rock mass

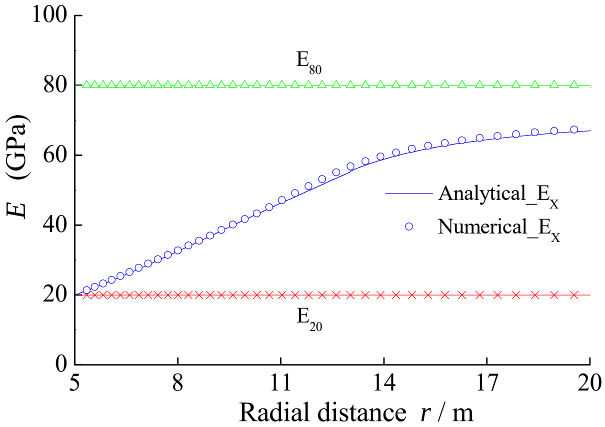

(a)

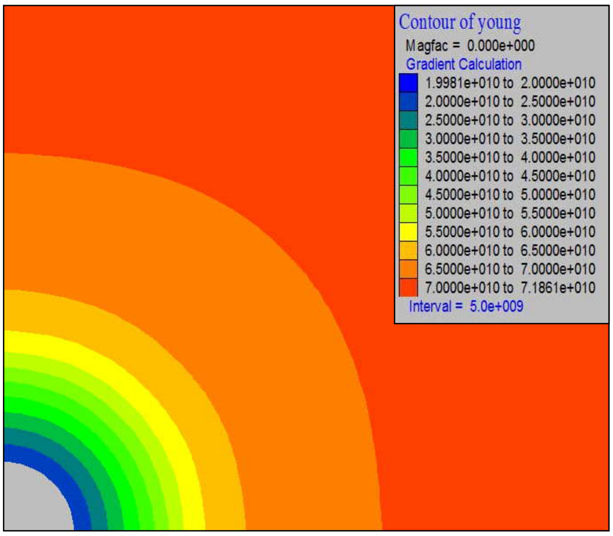

(b)

Fig. 6 The Young's modulus distributions in the surrounding rock mass (a) analytical results, (b) numerical results.

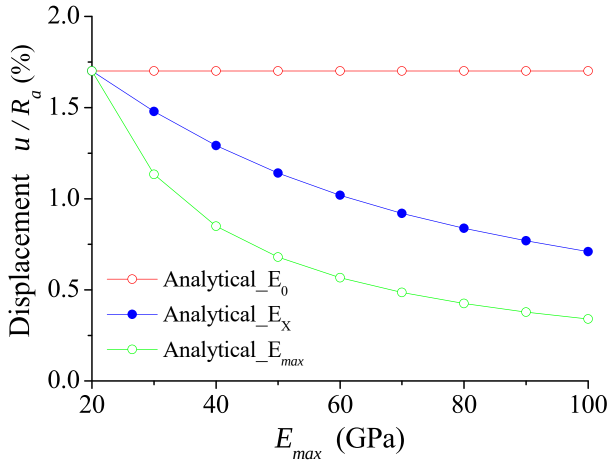

Fig. 7 The evolution of the maximum displacement with the increasing of E_{max}

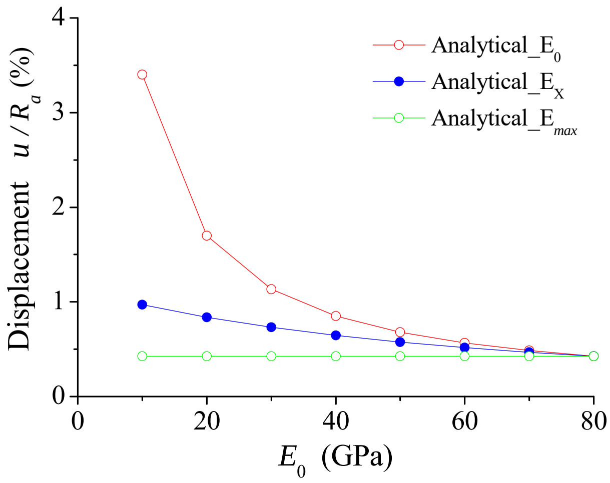

Fig. 8 The evolution of the maximum displacement with the increasing of E_0

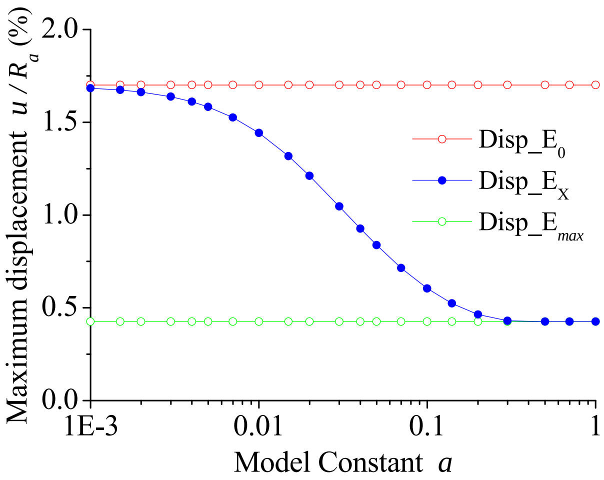

Fig. 9 The evolution of the maximum displacement and the error with the increasing of model constant

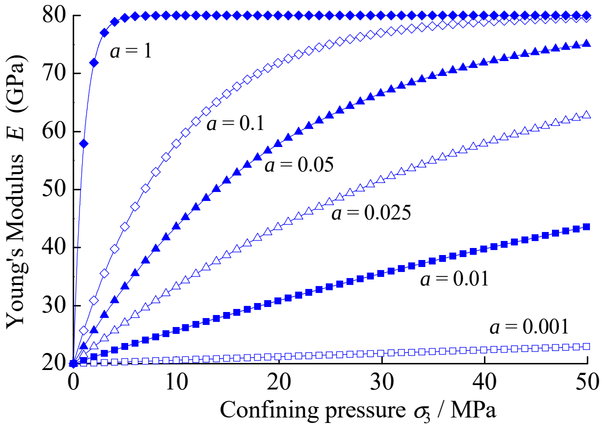

Fig. 10 The distribution of Young’s modulus with different value of model constant

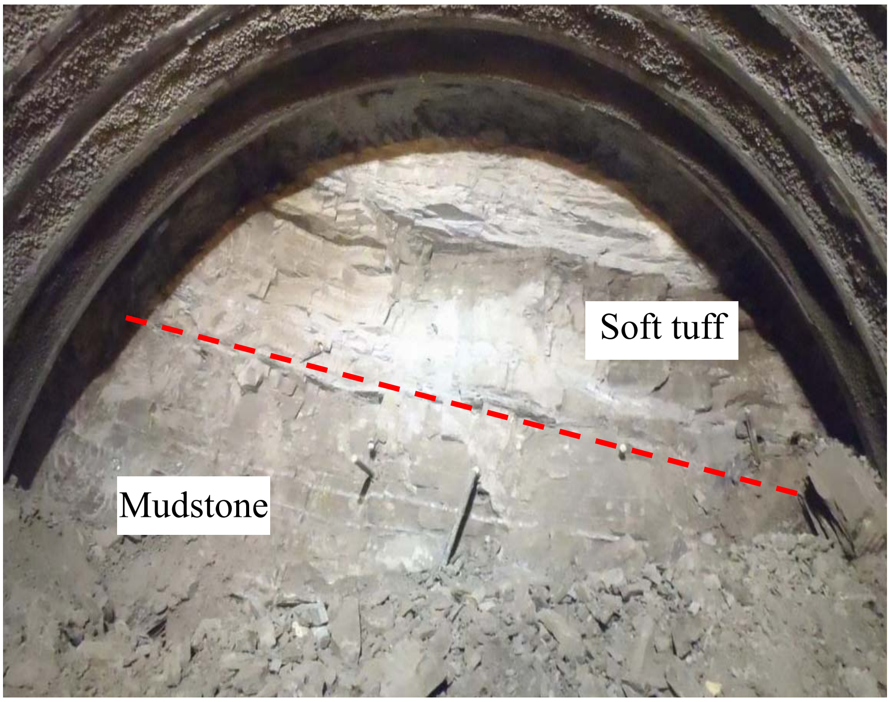

(a)

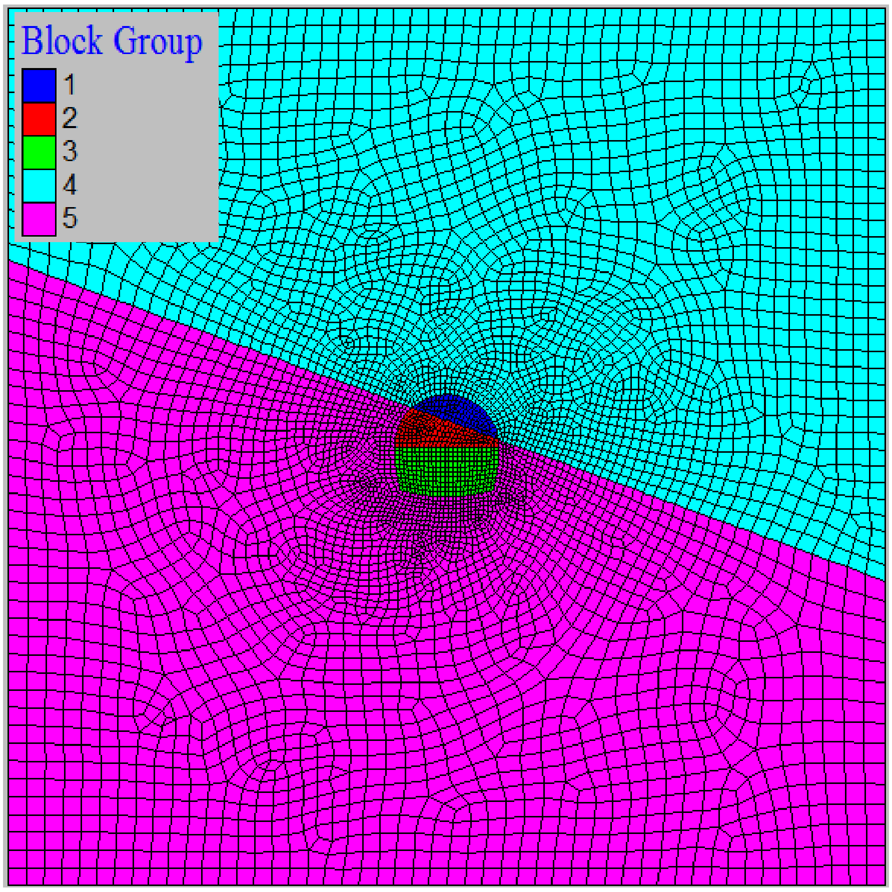

(b)

Fig. 11 Tawara saka Tunnel at 16.074km (a) The exposed tunnel face, (b) Numerical model

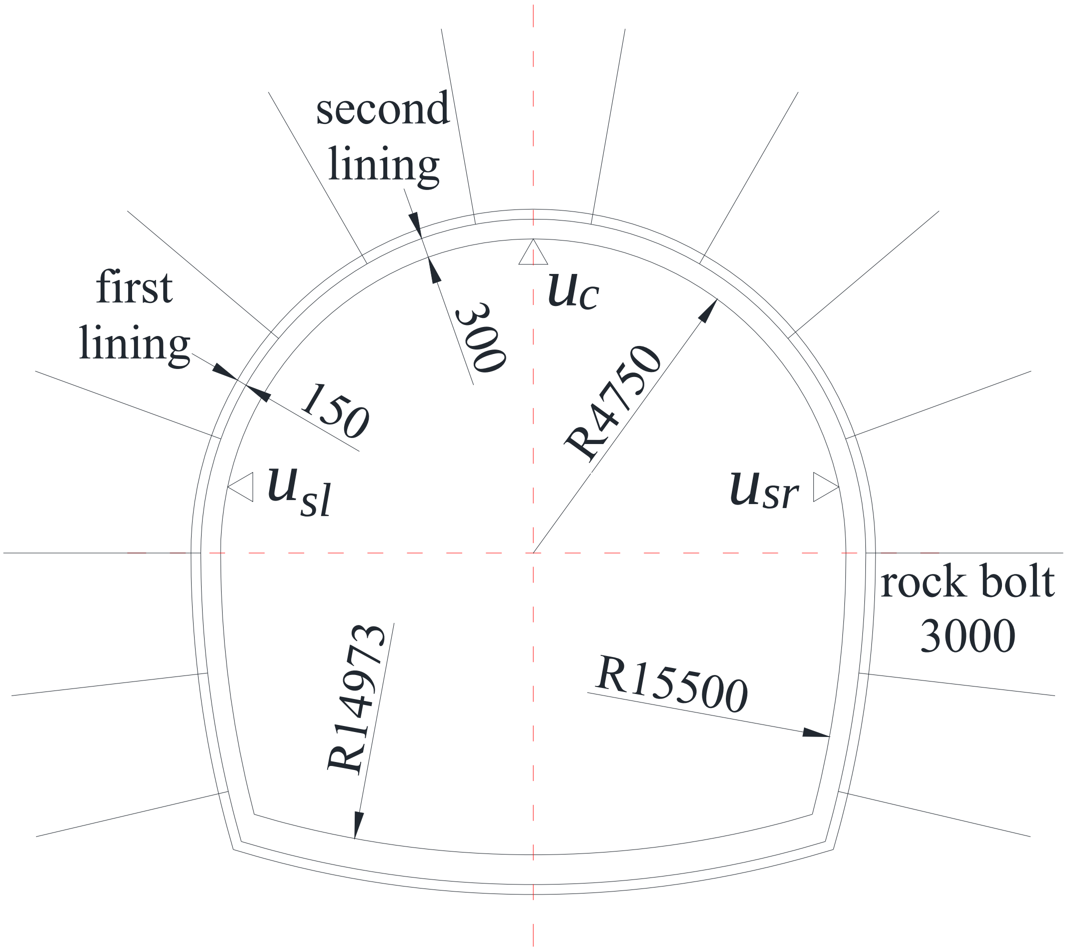

Fig. 12 The cross section dimensions and the convergence monitoring positions

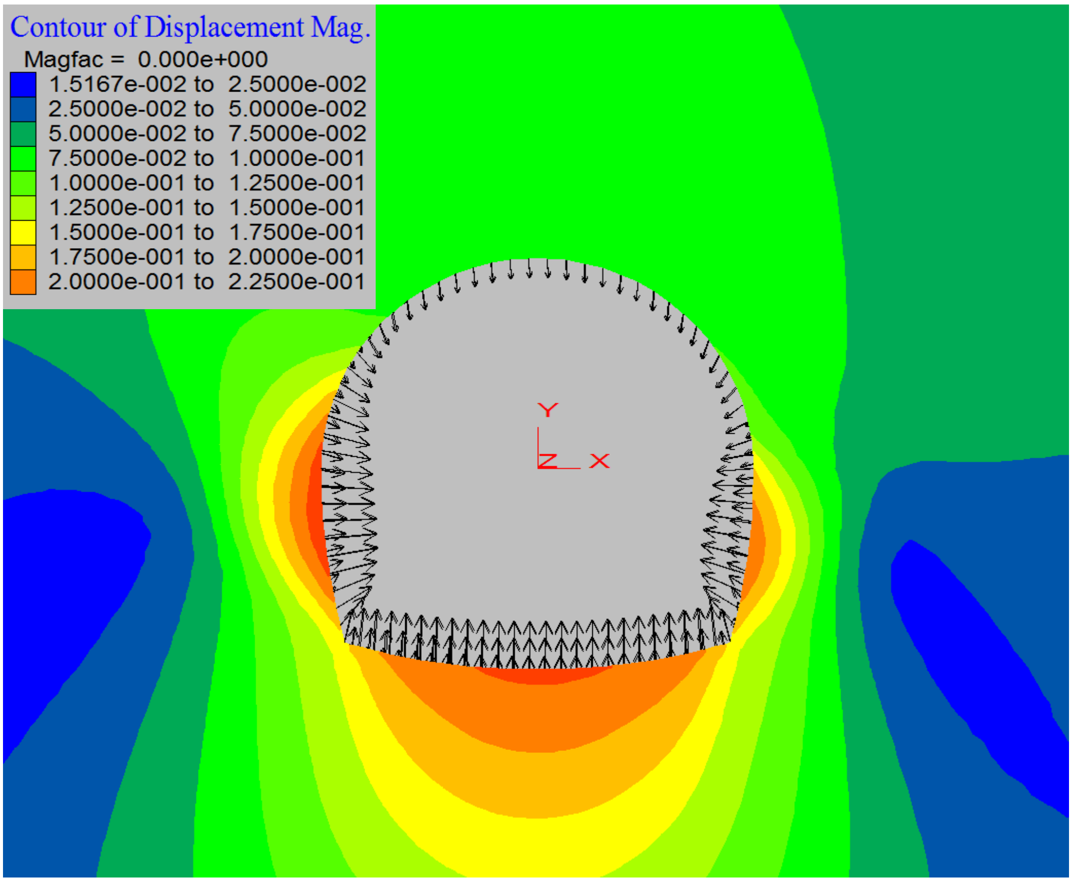

Fig. 13 Displacement of the rock mass around the tunnel by uniform Young's modulus model

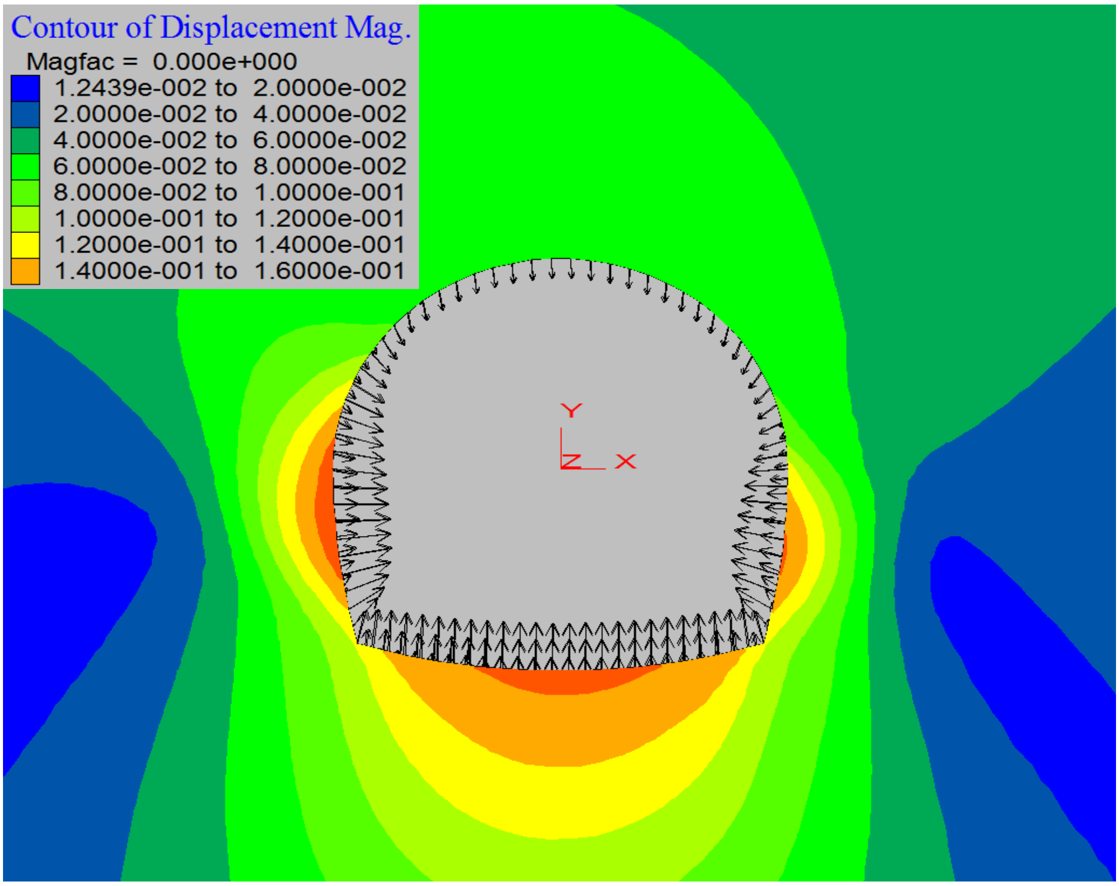

Fig. 14 Displacement of the rock mass around the tunnel by non-uniform Young's modulus model

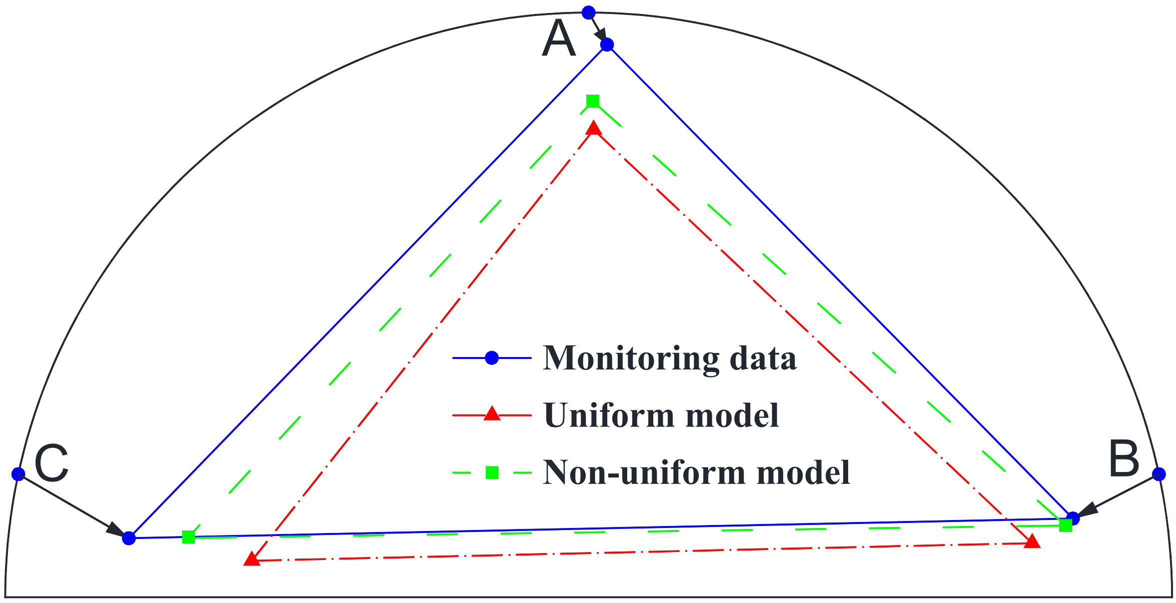

Fig. 15 Comparing of different numerical results with the monitoring data